arXiv:2009.09823v2 [cs.LG] 15 Aug 2021

Latent State Inference in a Spatiotemporal Generative Model*

Matthias Karlbauer[1][0000−0002−4509−7921], Tobias Menge[1], Sebastian Otte[1][0000−0002−0305−0463], Hendrik P. A. Lensch[2][0000−0003−3616−8668], Thomas Scholten[3][0000−0002−4875−2602], Volker Wulfmeyer[4][0000−0003−4882−2524], and Martin V. Butz[1][0000−0002−8120−8537]

[1] University of Tübingen – Neuro-Cognitive Modeling Group, Sand 14, 72076 Tübingen, Germany, martin.butz@uni-tuebingen.de

[2] University of Tübingen – Computer Graphics, Maria-von-Linden-Straße 6, 72076 Tübingen, Germany

[3] University of Tübingen – Soil Science and Geomorphology, Rümelinstraße 19-23, 72070 Tübingen, Germany

[4] University of Hohenheim – Institute for Physics and Meteorology, Garbenstraße 30, 70599 Stuttgart, Germany

Abstract. Knowledge about the hidden factors that determine particular system dynamics is crucial for both explaining them and pursuing goal-directed interventions. Inferring these factors from time series data without supervision remains an open challenge. Here, we focus on spatiotemporal processes, including wave propagation and weather dynamics, for which we assume that universal causes (e.g. physics) apply throughout space and time. A recently introduced DIstributed SpatioTemporal graph Artificial Neural network Architecture (DISTANA) is used and enhanced to learn such processes, requiring fewer parameters and achieving significantly more accurate predictions compared to temporal convolutional neural networks and other related approaches. We show that DISTANA, when combined with a retrospective latent state inference principle called active tuning, can reliably derive location-respective hidden causal factors. In a current weather prediction benchmark, DISTANA infers our planet's land-sea mask solely by observing temperature dynamics and, meanwhile, uses the self inferred information to improve its own future temperature predictions.

Keywords: Recurrent neural networks · graph neural networks · latent inference · weather prediction.

*Funded by the Deutsche Forschungsgemeinschaft (DFG, German Research Foundation) under Germany's Excellence Strategy - EXC number 2064/1 – Project number 390727645. Moreover, we thank the International Max Planck Research School for Intelligent Systems (IMPRS-IS) for supporting Matthias Karlbauer.

1 Introduction

When considering our planet's weather, centuries of past research have identified a large number of factors that affect its highly nonlinear and partially chaotic dynamics. Yet, can we ever be sure of having identified all hidden causal factors? Moreover, do we have (sufficient) data about them? These are fundamental questions in any prediction or forecasting task, including spatiotemporal processes such as soil property dynamics, traffic forecasting, energy-flow prediction (e.g in brains or supply networks), or recommender systems. Here, we investigate how unobservable hidden factors may be inferred from spatiotemporal data streams.

When regularities in hidden causes are detectable, they may be encoded in the latent activities of recurrent neural networks [18,20], such as a long short-term memory (LSTM) [10]. The involved and conventional forward-directed inference of recurrent neural networks, however, has two main disadvantages: First, the encodings of the hidden causes form while streaming data, meaning they are not available from the beginning of a sequence. Second, learning, detecting and shaping the encodings is relatively hard, because the error signal only decreases once the unfolding data stream is suitably compressed.

To overcome these limitations, we combine and extend the recently introduced DIstributed SpatioTemporal graph Artificial Neural network Architecture (DISTANA) [13] with active tuning (AT) [7,8,17], which facilitates the determination of hidden causal states via retrospective inference over time. Projected onto stable neural states, akin to parametric bias neurons [24,23], AT searches for constant input biases, assuming that the observed dynamics are influenced by particular constant and only indirectly observable factors.

Following the idea of *relational inductive biases* [3], DISTANA is designed to model the hidden causal processes that generate spatiotemporal dynamics. Hence, DISTANA assumes that the sensed dynamics are generated by universal causal principles (e.g. physics). Moreover, we endow DISTANA with the expectation that constant, hidden factors modify the spatiotemporal processes locally. For example, weather dynamics follow the universal principles of thermodynamics from physics and are locally dependent on the topology.

The contributions we make are as follows: (A) the combination of DISTANA with active tuning (AT) to infer constant, hidden factors locally, even when these factors are never made available to the network – neither as input nor as (target) output. (B) we show that reasonable latent neural activities are inferred during training and testing via retrospective spatiotemporal analysis. (C) after having learned a distributed, generative model of the globally unfolding dynamics, we demonstrate that our planet's land-sea mask as well as other causal factors can be inferred via the retrospective analysis of unfolding weather dynamics – partially again even when the algorithm was never informed about these factors – to increase the model's prediction abilities.

We conclude that the retrospective inference of latent states via AT offers a promising method to identify hidden factors in data streams, and that graph neural networks (GNN) like DISTANA bear great potential at modeling real-world spatiotemporal processes.

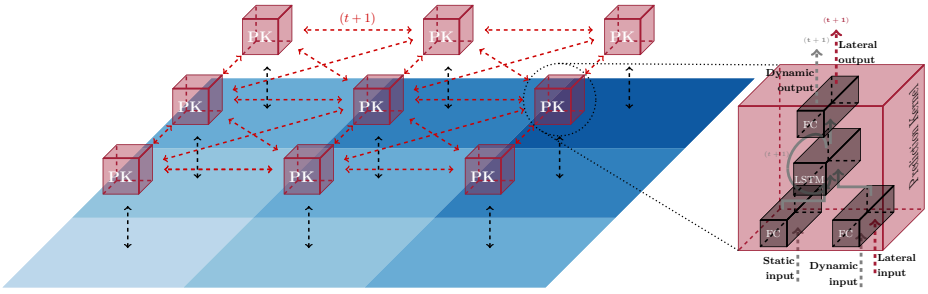


Fig. 1. 3×3 sensor mesh grid showing the connection scheme of Prediction Kernels (PKs) that model the local dynamical process while communicating laterally. Figure modified from [14].

2 DISTANA

As introduced in [13] and following the naming convention of [27], DISTANA (the DIstributed SpatioTemporal graph Artificial Neural network Architecture) can be described as a spatiotemporal graph neural network (ST-GNN). While GNNs give the designer a large amount of freedom in controlling the flow of information within the model (referred to as relational inductive biases) [3], they are reported to model physical systems with very high precision and accuracy for up to several hundreds of time steps even during closed loop prediction [2,22,16,21,25]. Thorough surveys about GNNs and the numerous ways of creating the graph and setting up the connection schemes are written by [6,3,27].

The GNN used in this work, DISTANA, consists of prediction kernels (PKs), which are arranged in a lattice structure. PKs model local dynamics concurrently. In every time step t, each PK receives (i) local dynamic data, and (ii) lateral output activities from the neighboring PKs from $t-1$ to exchange information between PKs. Here, we extend the PKs to (iii) additionally receive location specific static inputs. The time recurrent PKs process this information, combine it with their previous latent state, and generate (i) predictions of the next local dynamic data input at $t+1$, as well as (ii) outputs to the laterally connected PKs (cf. Figure 1). PKs are akin to a spatiotemporal convolutional kernel, since all PKs share identical weights, that is, a single set of weights is applied and optimized in every grid cell. As a result, the likelihood of overfitting local data irregularities is reduced and the emergence of a highly generalizing and universally applicable set of weights is fostered. Because of the reduction of trainable weights, less data is needed for training.

2.1 Alternative State-of-the-Art Architectures

We compared DISTANA with two well-suited deep learning approaches. First, we tested convolutional long short-term memory models (ConvLSTMs) [28] to predict circular wave dynamics (see Figure 2). The used ConvLSTM model has

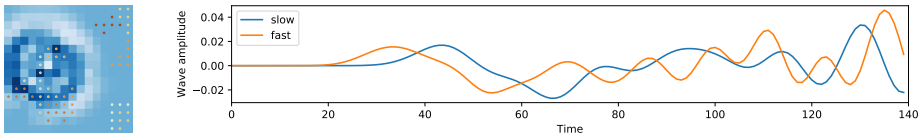


Fig. 2. Left: two-dimensional wave propagating through a 16×16 grid with obstacles. Darker dots in the grid nodes correspond to stronger blocking effect on the wave. Right: wave activity for two exemplary positions in the grid, with fast and slow propagation speeds.

2 952 free parameters to project the $16 \times 16 \times 1$ input (ignoring batch and time dimensions) via the first layer on eight feature maps (resulting in dimensionality $16 \times 16 \times 8$) and subsequently via the second layer back to one output feature map. All kernels have a filter size of $k = 3$, apply zero-padding and are implemented with a stride of one. The code was taken and adapted from[5]. Second, we tested Temporal Convolution Networks (TCN) [12,9,1]. The TCN used in this work is a three-layer network with 2 306 parameters, where the input layer projects to eight feature maps, which project their values back to one output value. A kernel filter size of $k = 3$ is used for the two spatial dimensions in combination with the standard dilation rate of $d = 1, 2, 4$ for the temporal dimension, resulting in a temporal horizon of 28 time steps, cf. [1]. Various experiments with other sizes and deeper network structures have not yielded any better performance than the one reported. Code was taken and adapted from [1].

2.2 Static Input Inference via Active Tuning

Essentially, active tuning (AT) [7,8,17] can be seen as a different paradigm for handling RNNs: instead of the usual input → compute → output scheme, a subset of the RNN's neurons is decoupled from the direct input signal. The activation of this subset of neurons is computed from the RNN's prediction-based gradients, both during training and testing. Gradient information is obtained from backpropagating the discrepancy between the RNN's predicted output $\hat{\mathbf{y}}$ and the desired output $\mathbf{y}$. Thus, the neuron dynamics of the subset is solely influenced by the target indirectly, by means of temporal gradient information induced by the prediction error.

In this work, as mentioned before, DISTANA receives dynamic and lateral input, while the static input $\mathbf{s}$ is withheld and must be inferred via AT to reasonably model the unfolding dynamics. Technically, $\mathbf{s}$ is fed to the model initially as a zero vector and optimized iteratively through the AT method. AT is applied to reduce local prediction errors, while the PK weights are updated as usual to reduce global prediction errors and model universal dynamics.

The active tuning algorithm, please refer to [17] for more information, can be applied in combination with any desired gradient optimization strategy, e.g.

[5] https://github.com/ndrplz/ConvLSTM_pytorch

Adam [15]. Furthermore, an arbitrary number of optimization cycles c, here $c = 1$, and history length H, here $H = 10$, can be chosen, where the latter indicates up to what time in the local past the latent context vector $\mathbf{s}$, which is assumed to be constant, is optimized. The AT optimization procedure is realized every ten time steps retrospectively on the predicted dynamic input, starting from time step τ to find a converging $\mathbf{s}$.

We have modified (AT) for application on two-dimensional data in order to infer an individual, slowly changing local latent variable, denoted as $\mathbf{s}_i$, for each vertex of the two-dimensional grid. AT so far has been applied to one-dimensional time series prediction for the inference of rarely changing contextual [7,8] or dynamically changing latent states [17]. In contrast to previous applications of AT, the inferred local static input $\mathbf{s}$ is not reset between sequences during training here, assuming a constant static context.

In our initial experiments, the inferred static input frequently drifted or potentially exploded, comparable to an Intern Covariate Drift [11]. We solve this problem, similarly to [11], by normalizing the inferred latent variable (in our case the static input $\mathbf{s}$), via the mean μ_s and standard deviation σ_s with respect to all inferred static inputs $\{s_i^t\}_{i=1}^k$, where k is the number of cells or pixels in the two-dimensional field. Additionally, to remove noise from the inference process caused by inconsistent gradient signals before and after the normalization, the weights W and the bias neuron b of the static input preprocessing layer are modified such that the activation of the static input preprocessing layer remains the same before and after the normalization:

$$b \leftarrow b + W \cdot \mu_s; \qquad W \leftarrow W \cdot \sigma_s \tag{1}$$

While the activation of the network is preserved, the gradients backpropagated through the static input preprocessing layer are affected asymmetrically by the modified weights and bias. In our experiments, this has been shown to substantially improve both the inference during training and the convergence of the inference process during testing.

3 Experiments and Results

The experiments are based on two classes of spatiotemporal time series. Both are representatives of universal, but locally and temporally modifiable, spatiotemporal, causal processes that propagate dynamics over local topologies throughout a homogeneously connected graph.

3.1 2D Circular Wave

Following [13], a spatiotemporal wave propagation dataset was created to validate our approach. In comparison to [13], however, the data generation was enhanced such that the wave propagation velocity could be contextually modified locally, which intuitively resembles obstacles in the water, which affect the wave's propagation behavior (cf. Figure 2).

This benchmark was used to (a) demonstrate and compare DISTANA's principal capability to model locally parameterized spatiotemporal dynamics and (b) determine whether DISTANA can be used in combination with AT to infer an underlying and hidden static (causal) factor, which modifies the observed dynamics locally. Adam [15] is used for training with a learning rate of 10^{-3} along with Scheduled Sampling [4] with a linear slope of 270 epochs, transitioning from a probability of $0.0 \rightarrow 0.9$ of feeding the network with its own output in the next iteration instead of the teacher signal. During each sequence, 30 teacher forcing steps are conducted to induce reasonable network activities before switching to closed loop. Network inputs $\mathbf{x}$ and the according targets $\mathbf{y}$ are exactly the same sequences shifted by one time step to train four different model types (ConvLSTM, TCN, DISTANA and DISTANA + AT) to iteratively predict the next two-dimensional dynamic wave field state (one step ahead prediction). For the static input inference, DISTANA is augmented with a parametric bias neuron, whose activity is inferred during training and testing, aiming at the identification of an unknown location-specific wave velocity-influencing factor (static context). Training was realized over 300 epochs consisting of 100 training sequences of length 120 each. The target static context vector $\mathbf{s} \in \mathbb{R}^{16\times16}$ was initialized by drawing values from $\{0.2, 0.3, 0.5, 0.6, 0.8, 0.9\}$, where small values cause the waves to propagate slower at the according pixel. An exemplary ground truth context map $\mathbf{s}_{GT}$ is visualized in Figure 2 (left, brownish dots). Note that $\mathbf{s}_{GT}$ was used for the data generation but has never been provided to any model. The preprocessing layer size of DISTANA was set to eight neurons and the subsequent LSTM layer consisted of twelve cells, yielding 1 236 parameters. For the DISTANA + AT model, an additional static preprocessing layer with five neurons was used, resulting in 1 486 weights overall, compared to 2 952 and 2 306 weights for ConvLSTM and TCN, respectively.

To test the models' generalization capabilities, 16 new static context vectors $\mathbf{s}'$ have been generated by drawing from $\{0.2, 0.3, \ldots, 1.0\}$ (e.g. see Figure 3, top right-most). All models were evaluated on 50 sequences – made up of 120 time steps each – per $\mathbf{s}'$. Reasonable activity was induced into the models by applying 30 steps of teacher forcing, followed by 90 steps of closed loop prediction for which an average MSE over all test examples and spatial locations was computed. For DISTANA + AT, the static context has been inferred before the testing on 50 separate sequences, using a history length of $H = 30$, one optimization cycle ($c = 1$), and an inference learning rate of $\eta = 0.1$ for the first three epochs, and $\eta = 0.01$ for the remaining seven epochs.

3.2 2D Circular Wave Results

The prediction accuracy of ConvLSTM, TCN, DISTANA and DISTANA + AT differs considerably. TCN without scheduled sampling tends to start oscillating increasingly after few steps of closed loop prediction, resulting in a mediocre MSE score of $(2.94 \pm 2.38) \times 10^{-2}$, while ConvLSTM $(8.69 \pm 0.87) \times 10^{-4}$ and DISTANA $(8.69 \pm 0.87) \times 10^{-4}$, both trained with scheduled sampling, tend to vanish after few steps of closed loop prediction. Solely DISTANA + AT trained

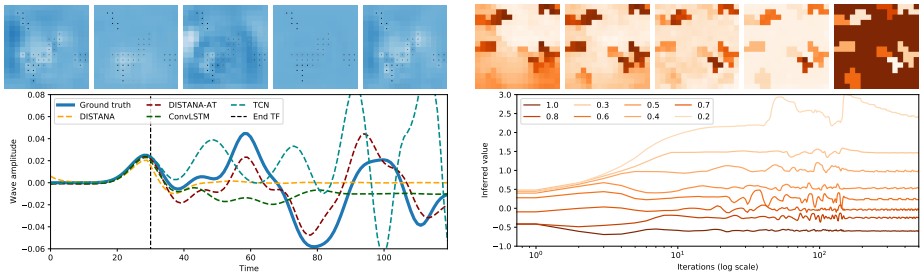


Fig. 3. Top left: ground truth and model outputs at time step 80, which is 30 time steps after the start of closed loop prediction (from left to right: ground truth, ConvLSTM, TCN, DISTANA, DISTANA + AT). Bottom left: ground truth and model outputs over time at position $x = 2$, $y = 6$ in the two-dimensional grid. Top right: inferred static context during testing with values in the range $[-0.6, 2.6]$ after 1, 2, 10, 500 iterations and ground truth with values in $[0.0, 1.0]$. For the ground truth, darker color corresponds to a stronger blocking effect on the wave, which was learned and inferred inversely by the network. Bottom right: average inferred contexts over time during testing (x-axis log scaled).

with scheduled sampling is able to preserver a stable activation pattern with an MSE of $(3.87 \pm 2.48) \times 10^{-4}$.

Furthermore, as shown in Figure 3 (bottom right), DISTANA + AT preserves a linear ordering when inferring context values that were never encountered during training as indicated by the static context values 0.4 and 0.7, which are properly mapped to roughly -0.1 and -1.1, respectively, without violating the propagation speed order with respect to other static context values. Thus, looking at the estimated static context $\hat{\mathbf{s}}$, it turns out that the latent state inferred by AT correctly reproduced the monotonicity of the here known underlying structure. The static context map at test time, which is different to the map on which the model was trained on, is inferred correctly (see image sequence of Figure 3, top right). When comparing the prediction accuracy of DISTANA and DISTANA + AT in Figure 3 (top and bottom left), the self-inferred static context clearly helps DISTANA + AT to model the two-dimensional wave.

3.3 WeatherBench

Recently, [19] introduced a benchmark for comparing mid-range (that is three to five days) weather forecast qualities of data driven and physics-based approaches. While globally regularly aggregated data are provided in three spatial resolutions (5.625°, 2.8125° and 1.40525° resulting in 32×64, 64×128 and 128×256 grid points, respectively), evaluated baselines are reported for the coarsest resolution only, which in consequence we chose too for elaborating and comparing DISTANA. Baselines are generated by means of persistence (tomorrow's weather is today's weather), climatology, linear regression, and physics-based numerical weather prediction models. Moreover, convolutional neural networks (CNNs) are either applied iteratively or directly. Baselines are computed solely on three or five

day predictions of the geopotential at an atmospheric pressure level of 500 hPa (roughly at 5.5 km height, called Z500) and the temperature at 850 hPa (∼1.5 km height, referred to as T850). Beyond Z500 and T850, weatherBench consists of numerous additional dynamic variables (humidity, precipitation, wind direction and speed, solar radiation, etc.), partially reported on multiple vertical layers, and static variables (land-sea mask, soil type, orography, latitude and longitude).

We use weatherBench (a) to explore DISTANA's abilities to approximate real-world phenomena by comparing it to [19]'s iterative CNN approach and (b) to investigate how to apply gradient-based inference techniques in order to infer local static context (e.g. the land-sea mask) that affect Z500 and T850. The experiments we conducted on weatherBench focused on the prediction of the Z500 (geopotential) and T850 (temperature) variables. DISTANA and DISTANA + AT were trained for 2 000 epochs on weather data from 1979, using a learning rate of 10^{-4}, validated on 2016, and tested on 2017. Each year was partitioned into sequences of 96 hourly steps, yielding 91 sequences per year. Increasing the set sizes or changing the training, validation, or testing years did not seem to alter the results or model performances. DISTANA's preprocessing and LSTM layers were set to 50 neurons and cells, respectively. Furthermore, the implementation of DISTANA was enhanced to support a varying lateral communication vector size, which then was increased from one to five neurons, to enable neighboring PKs to exchange information of higher complexity, yielding $\sim 25\,000$ parameters, slightly varying with the number of input variables. Moreover, the lateral connection scheme of DISTANA was specified such that information exiting the horizontal boundaries would enter at the other end of the field to match weatherBench's horizontally connected spherical data composition.

Selected static information provided by weatherBench was adapted and extended to facilitate the learning process. Changes were made to the latitude and longitude variables: latitude was transformed to be zero at the equator and non-linearly rising to one towards the poles, based on cos(lat). The longitude variable was split into its sine and cosine component, creating a circular encoding to match the spherical shape of the Earth from which the data origins. Additionally, one-dimensional north- and south-flags were provided to account for the missing neighbors in the north- and south-most rows in the grid. As has been done in [26], we also provide the top of atmosphere total incident solar radiation (tisr). All variables were normalized to the range of $[-1.0, 1.0]$. When using AT to infer a latent static context $\tilde{\mathbf{s}}$, the values were clamped to $[-1.0, 1.0]$ to prevent them from drifting or exploding. If not specified differently, we provide the models with the dynamic variable Z500 or T850 (being subject for prediction), along with nine static inputs: orography, land-sea mask (LSM), soil type, longitude (two-dimensional), latitude, tisr, and the north- and south-end flags.

3.4 WeatherBench Results

The evaluation of DISTANA being trained to predict the Z500 variable for a lead time of 72 h yielded an RSME of 816, which is better than the current best comparable iterative approach reported on the benchmark (RMSE = 1114).

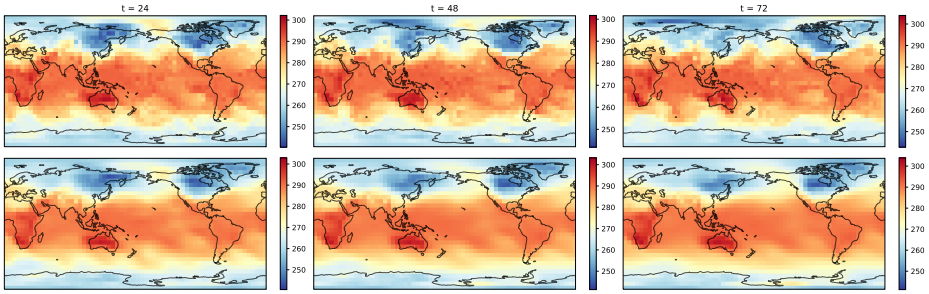


Fig. 4. Predicted temperature (T850) in degree Kelvin for 24, 48 and 72 hours (corresponding to time steps) into the future (closed-loop). The first row shows the ground truth and the second row the network output.

However, seeing that the best numerical operational weather prediction model produces an RMSE of 154 and other machine learning approaches achieve an RMSE of 268, there is certainly room for improvement. Nonetheless, DISTANA offers the best learned generative, iterative processing model on the benchmark without applying techniques that reduce the distortion resulting from transforming the spherical Earth data to a regular two-dimensional grid.

A second experiment was conducted to (a) investigate whether DISTANA + AT is able to predict the T850 variable, see Figure 4, and (b) simultaneously infer missing land-sea mask (LSM) values only from the observed T850 dynamics. The model thus received the same static input as in the previous experiment along with the T850 variable during training. However, only two thirds of the LSM values were provided. The other third, considered missing values, which covered America and the Atlantic ocean, were to be inferred. After training, the entire LSM vector $\hat{\mathbf{s}}_{\text{LSM}}$, initialized with zeros, was retrospectively tuned via AT such that it would best explain the observed dynamics. As visualized in Figure 5 (top center) the missing LSM is inferred reasonably, including the American continent, which the network has never seen during training or inference. These findings suggest that the model learned a generalizable, globally applicable encoding of the LSM's influence on the T850 dynamics.

In a third experiment, we used an additional latent neuron – a parametric bias neuron – that is locally tuned during training via AT. This latent neuron is supposed to be tuned freely by the model to develop any code that helps the model to predict the observed dynamics. We were particularly interested in evaluating whether DISTANA would develop latent states $\tilde{\mathbf{s}}$ that distinctively encode prediction-relevant, hidden causal factors that correspond to observable values. For example, we wanted to see whether DISTANA would develop a latent code that resembles any land-coding quantity. Thus, in this experiment, we try to answer the question what latent states are inferred depending on the predicted variable and how the presence of land-relevant input does affect the generation of this latent code.

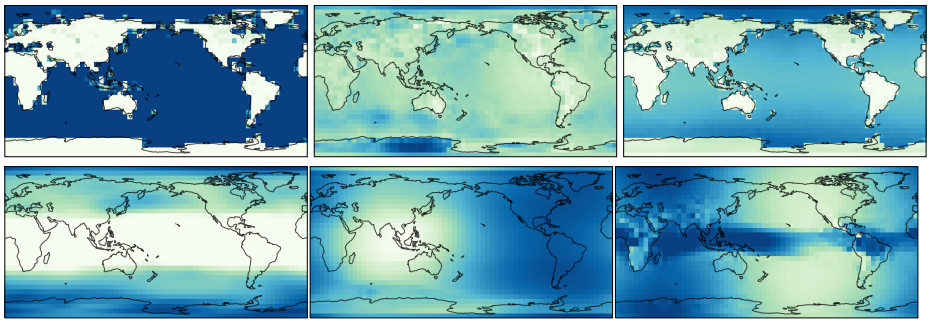


Fig. 5. Top left: original land-sea mask (LSM). Top center: global LSM inferred during testing after being trained on two thirds of the globe (the model has never seen America's LSM). Top right: a latent vector which developed during training and encodes LSM information as well as a decent latitude coding. Bottom: three latent variable codes that freely emerged during training of the Z500 (left, center) and T850 (right) variables.

Our results indicate that the nature of the developed latent states depends considerably on both the variable that is subject for prediction (Z500 or T850) and the additional static data provided. Figure 5 (top right) shows a clear tendency to encode land-sea information, augmenting it with a latitude code, when all previously mentioned static inputs (including LSM) were provided. When training a model to predict Z500, the emerging latent variables rather seem to encode latitude, albedo, monsoon [5], or humidity-distribution patterns (Figure 5 bottom left and center). Excitingly, nuances of LSM and orography become visible when training to predict T850 without receiving any land-coding inputs (see Figure 5 bottom right). Nevertheless, further studies are necessary to verify to which extent the inferred variables correlate with observations in detail.

4 Final Discussion

The presented results indicate that the combination of the DIstributed, SpatioTemporal graph Artificial Neural network Architecture, DISTANA, with the retrospective inference mechanism called active tuning (AT), bears large potential at predicting spatiotemporal real-world phenomena (e.g. weather). It outperforms competing deep learning algorithms by generating more accurate closed-loop predictions into the future. In addition, it can infer hidden causes by mere observation of a dynamic process. In particular, AT in DISTANA is well-suited for inferring (i) contrastive hidden causes during learning and (ii) hidden static activities while minimizing loss online. While we believe that these hidden factors tend to identify causal influences – because they form for improving the accuracy of the predicted dynamics – future research will need to investigate the robustness of this tendency.

During learning, cumulative error signals in latent parametric bias neurons at the individual prediction kernels tend to develop encodings of hidden, dynamic-

influencing factors. To a certain extent, these neuronal encodings resemble physical properties, such as albedo or the land-sea mask, depending on the type of dynamics that is to be predicted (e.g. temperature or geopotential). That is, the projection of the gradient onto static neural activities identifies local parametric bias activities that best characterize local, hidden causal factors.

Overall, the results suggest that our approach of assuming and inferring hidden causes with constrained properties – such as being locally distinct, constant, but universally present – offers strong potential in fostering the development of process-explaining structures.

References

1. Bai, S., Kolter, J.Z., Koltun, V.: An empirical evaluation of generic convolutional and recurrent networks for sequence modeling. arXiv:1803.01271 (2018)
2. Battaglia, P., Pascanu, R., Lai, M., Rezende, D.J., et al.: Interaction networks for learning about objects, relations and physics. In: Advances in neural information processing systems. pp. 4502–4510 (2016)
3. Battaglia, P.W., Hamrick, J.B., Bapst, V., Sanchez-Gonzalez, A., Zambaldi, V., Malinowski, M., Tacchetti, A., Raposo, D., Santoro, A., Faulkner, R., et al.: Relational inductive biases, deep learning, and graph networks. arXiv:1806.01261 (2018)
4. Bengio, S., Vinyals, O., Jaitly, N., Shazeer, N.: Scheduled sampling for sequence prediction with recurrent neural networks. arXiv:1506.03099 (2015)
5. Boers, N., Goswami, B., Rheinwalt, A., Bookhagen, B., Hoskins, B., Kurths, J.: Complex networks reveal global pattern of extreme-rainfall teleconnections. Nature **566**(7744), 373–377 (2019)
6. Bronstein, M.M., Bruna, J., LeCun, Y., Szlam, A., Vandergheynst, P.: Geometric deep learning: going beyond euclidean data. IEEE Signal Processing Magazine **34**(4), 18–42 (2017)
7. Butz, M.V., Bilkey, D., Humaidan, D., Knott, A., Otte, S.: Learning, planning, and control in a monolithic neural event inference architecture. Neural Networks **117**, 135–144 (2019)
8. Butz, M.V., Menge, T., Humaidan, D., Otte, S.: Inferring event-predictive goal-directed object manipulations in reprise. Artificial Neural Networks and Machine Learning – ICANN 2019 **11727**, 639–653 (2019)
9. Dauphin, Y.N., Fan, A., Auli, M., Grangier, D.: Language modeling with gated convolutional networks. In: Proceedings of the 34th International Conference on Machine Learning-Volume 70. pp. 933–941. JMLR. org (2017)
10. Hochreiter, S., Schmidhuber, J.: Long short-term memory. Neural computation **9**(8), 1735–1780 (1997)
11. Ioffe, S., Szegedy, C.: Batch normalization: Accelerating deep network training by reducing internal covariate shift. In: Bach, F., Blei, D. (eds.) Proceedings of the 32nd International Conference on Machine Learning. Proceedings of Machine Learning Research, vol. 37, pp. 448–456. PMLR, Lille, France (07–09 Jul 2015)
12. Kalchbrenner, N., Espeholt, L., Simonyan, K., Oord, A.v.d., Graves, A., Kavukcuoglu, K.: Neural machine translation in linear time. arXiv:1610.10099 (2016)
13. Karlbauer, M., Otte, S., Lensch, H.P.A., Scholten, T., Wulfmeyer, V., Butz, M.V.: A distributed neural network architecture for robust non-linear spatio-temporal prediction. arXiv:1912.11141 (12 2019)

14. Karlbauer, M., Otte, S., Lensch, H.P., Scholten, T., Wulfmeyer, V., Butz, M.V.: Inferring, predicting, and denoising causal wave dynamics. In: International Conference on Artificial Neural Networks. pp. 566–577. Springer (2020)
15. Kingma, D., Ba, J.: Adam: A method for stochastic optimization. International Conference on Learning Representations (12 2014)
16. Kipf, T., Fetaya, E., Wang, K.C., Welling, M., Zemel, R.: Neural relational inference for interacting systems. arXiv:1802.04687 (2018)
17. Otte, S., Karlbauer, M., Butz, M.V.: Active tuning. arXiv:2010.03958 (2020)
18. Rabinowitz, N., Perbet, F., Song, F., Zhang, C., Eslami, S.M.A., Botvinick, M.: Machine theory of mind. In: Dy, J., Krause, A. (eds.) Proceedings of the 35th International Conference on Machine Learning. Proceedings of Machine Learning Research, vol. 80, pp. 4218–4227. PMLR, Stockholm Sweden (10–15 Jul 2018)
19. Rasp, S., Dueben, P.D., Scher, S., Weyn, J.A., Mouatadid, S., Thuerey, N.: Weatherbench: A benchmark dataset for data-driven weather forecasting. arXiv:2002.00469 (2020)
20. Rodriguez, R.C., Alaniz, S., Akata, Z.: Modeling conceptual understanding in image reference games. In: Advances in Neural Information Processing Systems. pp. 13155–13165 (2019)
21. Sanchez-Gonzalez, A., Heess, N., Springenberg, J.T., Merel, J., Riedmiller, M., Hadsell, R., Battaglia, P.: Graph networks as learnable physics engines for inference and control. arXiv:1806.01242 (2018)
22. Santoro, A., Raposo, D., Barrett, D.G., Malinowski, M., Pascanu, R., Battaglia, P., Lillicrap, T.: A simple neural network module for relational reasoning. In: Advances in neural information processing systems. pp. 4967–4976 (2017)
23. Sugita, Y., Tani, J., Butz, M.V.: Simultaneously emerging braitenberg codes and compositionality. Adaptive Behavior **19**, 295–316 (2011)
24. Tani, J., Ito, M., Sugita, Y.: Self-organization of distributedly represented multiple behavior schemata in a mirror system: Reviews of robot experiments using rnnpb. Neural Networks **17**, 1273–1289 (2004)
25. Van Steenkiste, S., Chang, M., Greff, K., Schmidhuber, J.: Relational neural expectation maximization: Unsupervised discovery of objects and their interactions. arXiv:1802.10353 (2018)
26. Weyn, J.A., Durran, D.R., Caruana, R.: Improving data-driven global weather prediction using deep convolutional neural networks on a cubed sphere. arXiv:2003.11927 (2020)
27. Wu, Z., Pan, S., Chen, F., Long, G., Zhang, C., Yu, P.S.: A comprehensive survey on graph neural networks. arXiv:1901.00596 (2019)
28. Xingjian, S., Chen, Z., Wang, H., Yeung, D.Y., Wong, W.K., Woo, W.c.: Convolutional LSTM network: A machine learning approach for precipitation nowcasting. In: Advances in neural information processing systems. pp. 802–810 (2015)